

APPLICATION OF DYNAMIC MANIPULATION OF THE FOREBODY VORTICES ON A SCHEMATIC AIRCRAFT MODEL

R. Lee* , R. J. Kind†
 Carleton University, Ottawa, Canada

E. S. Hanff‡
 National Research Council, Ottawa, Canada

Keywords: *high angle of attack, asymmetric forebody vortices, dynamic manipulation, duty cycle*

Abstract

Wind-tunnel tests have been conducted to further explore the potential of dynamic manipulation of forebody vortices as a means of augmenting directional control of fighter aircraft at high angles of attack. Tests were conducted on an aircraft model having a 65-deg delta wing and a slender, pointed forebody. Two forward-blowing nozzles located near the apex of the forebody served as the means of perturbing the forebody vortices. Blowing is alternated between the two nozzles causing the vortices to switch back and forth between their two asymmetric stable arrangements. It was found that time-average yawing moment can be made to vary linearly between the two extreme values arising from these orientations. The behaviour of other aerodynamic coefficients is also influenced. A peculiar reversal of yawing moment occurs when the blowing momentum exceeds a particular threshold value. Varying the longitudinal and circumferential location of the nozzle exits did not significantly change the control effectiveness.

*Graduate Student, Department of Mechanical and Aerospace Engineering.

†Professor, Department of Mechanical and Aerospace Engineering.

‡Senior Research Officer, Aircraft Dynamics Group, Aerodynamics Laboratory, Institute for Aerospace Research.

1 Nomenclature

b	wing span
c	mean geometric chord
\bar{C}_ℓ	time-average rolling moment coefficient, $(1/n \sum_1^n L)/q_\infty S b$
\bar{C}_m	time-average pitching moment coefficient, $(1/n \sum_1^n M)/q_\infty S c$
\bar{C}_n	time-average yawing moment coefficient, $(1/n \sum_1^n N)/q_\infty S b$
\bar{C}_Y	time-average side force coefficient, $(1/n \sum_1^n Y)/q_\infty S$
\bar{C}_Z	time-average normal force coefficient, $(1/n \sum_1^n Z)/q_\infty S$
C_μ	coefficient of blowing momentum, $\dot{m}_j V_j / q_\infty S$
d	nozzle diameter
D	base diameter of forebody
\dot{m}_j	nozzle mass flowrate, $\rho \pi d^2 V_j / 4$
n	number of sample points within an ensemble-averaged record
q_∞	freestream dynamic pressure, $\frac{1}{2} \rho V_\infty^2$
R	forebody cross-sectional radius at x_n
Re_D	Reynolds number, $V_\infty D / \nu$
S	wing reference area
T	period of the alternating blowing cycle
V_∞	freestream velocity
V_j	blowing velocity at nozzle exit
x_n	longitudinal location of nozzle exit relative to the nose apex
α	angle of attack
β	angle of sideslip

- θ azimuthal location of nozzle exit relative to the windward meridian
- τ duration a valve is open during the alternating blowing cycle
- ω angular frequency of alternating blowing
- ω^* reduced frequency of alternating blowing, $\omega D/V_\infty$

2 Introduction

The manipulation of forebody vortices is viewed as a means of augmenting directional control of high-performance aircraft required to perform maneuvers in the post-stall flight regime. The approach is attractive for flight control at high angles of attack because it permits the generation of large side forces and yawing moments when the vertical tail has lost its effectiveness.

Several techniques of manipulating the forebody vortices have been investigated [1, 2]. Most methods, however, are essentially steady schemes producing quasi-steady loads by forcing the forebody vortices into desired positions with respect to the forebody. To overcome the inherent bi-stability of forebody vortices over a significant range of angles of attack, steady methods involve first forcing the vortices to adopt a symmetrical stance, typically by choosing an appropriate forebody geometry. Desired side forces and yawing moments are then generated by coercing the vortices into an asymmetric orientation by either pneumatic or mechanical means. The need to overcome the artificially induced symmetry may require considerable control power. Furthermore, it is difficult to implement suitable control laws due to the severely non-linear response of the vortices, and thus resulting loads, to the control variable.

2.1 Principle of Dynamic Vortex Manipulation

A *dynamic* vortex control scheme has been developed which has shown the potential to overcome the aforementioned problems. The principle is illustrated in Fig. 1. Unlike the steady methods, this scheme takes advantage of the bi-stable nature of the forebody vortices and makes use of the

widely known fact that minute disturbances to the flow in the vicinity of the forebody tip can cause the forebody vortices to switch between their two stable states. Specifically, the scheme requires the forebody vortices to be deliberately switched, back and forth, between their stable states at a sufficiently high frequency such that the inertia of the aircraft prevents it from responding to the instantaneous loads. The aircraft would, however, respond to the time-average load which is controlled by varying the fraction (τ/T) of the switching-cycle period during which the vortices are in one state or the other. Load modulation is accomplished with intermittent perturbations of fixed intensity as opposed to variable intensity (of nozzle or slot flow rates, or strake deflection) required with steady schemes. Ideally the side force and yawing moment for steady port blowing ($\tau/T = 100\%$) would be equal and opposite to that for steady starboard blowing ($\tau/T = 0\%$). Then for oscillating blowing, the time-average side force and yawing moment would vary linearly with τ/T , being zero at $\tau/T = 50\%$, as shown in Fig. 1(b).

The deliberate flow perturbation can be implemented by either pneumatic or mechanical means.

2.2 Previous Work

The investigation of this vortex control scheme began with water-tunnel experiments[3]. The model used in these early experiments was an ogive-cylinder with an apex semi-angle of 30 deg. Hydrodynamic means were used to perturb the vortices by fitting the ogive-cylinder with two forward-facing, surface-flush nozzles symmetrically placed near the tip. ‘Blowing’ fluid could be supplied to either nozzle. By switching the blowing back and forth between the two nozzles it was found that very low blowing coefficients ($C_\mu = 0.0013$) were sufficient to reliably switch the forebody vortices from one stable configuration to the other at a reasonably high reduced frequency ($\omega^* = 0.16$). Having established that the forebody vortices respond to oscillatory forward-blowing, the next phase in the investigation was to determine the variation of the

time-average side force and yawing moment as a function of blowing duty cycle parameter, τ/T . Scaled up tests were performed in a wind tunnel using a version of the water-tunnel model[4]. Forward-blowing was again used as the perturbation method. Figure 2 shows the key results from these experiments. Note that time-average yawing moment and side force coefficients vary linearly with duty cycle for any particular angle of attack, α . Some non-linearity is present only for $\alpha=70$ deg. Note also, however, that the dependence on α is highly non-linear, reflecting the influence of α on the forebody vortex behaviour for steady or zero blowing. Both the magnitude of the side force and the position of the centre of pressure vary strongly with α .

The present paper is based on work performed in subsequent wind-tunnel tests using a schematic aircraft model. The main objective of these tests was to ascertain whether the excellent results obtained on the simple ogive-cylinder models could be replicated on a more realistic aircraft-like configuration.

3 Experimental Setup

The investigation was conducted in the $2\text{m} \times 3\text{m}$ low-speed, closed circuit wind tunnel at the National Research Council of Canada.

3.1 Model

The schematic aircraft model used in these experiments, Fig. 3, features a 65 deg delta-wing, vertical tail, and long, slender forebody. This model was originally designed for dynamic wind-tunnel experiments at high roll and pitch rates. The forebody of the model has a circular cross-section and a tangent-ogive profile with an apex semi-angle of 12.8 deg. Once again forward blowing was used as the vortex perturbation method. The forebody was designed to accept interchangeable tips so that a series of nozzle configurations could be readily tested. Emphasis was placed on locating the nozzle exits closer to the apex than in the previous tests in order to enhance blowing effectiveness. As shown in Fig. 4, the removable tip is 6.35cm long, containing symmetrically-

placed nozzles oriented parallel to the forebody axis of revolution. The nozzles have a diameter of 1.52mm ($d/D = 0.0191$), which was found to be the smallest possible size that could be drilled without significant deviation of the drill path.

The redesign of the forebody also involved the installation of a blowing system within its cavity. The system included two miniature solenoid on/off valves and two flow metering orifices to control and measure the air flow to each nozzle in the tip. A differential pressure transducer was placed across each metering orifice to measure the flow rate on the basis of a calibration of the pressure drop as a function of volume flow rate. The system was fed with regulated shop air via a supply tube carried inside the model support assembly and hollow balance. The valves were controlled by the data acquisition system.

3.2 Model Support

The model was sting-mounted on a vertical strut attached to turntables located at the floor and ceiling of the test section. The turntables were used to set the body inclination relative to the freestream, as shown in Fig. 5. The sting and model could be rolled such that combinations of turntable angle and model roll angle could produce a range of angles of attack and sideslip. An internal five-component balance (no axial force) measured aerodynamic forces and moments in the body axes. A blockage correction was applied to the dynamic pressure using the simple 1/4-area ratio[5].

3.3 Data Acquisition

Balance and pressure data (from the nozzle blowing system) was acquired by a computer with a high-performance digital signal processing (DSP) module. The DSP module included a 16-channel A/D converter board with a sampling rate of 150 kHz per channel. Ten channels were used to acquire balance data, pressure data and the valve drive waveforms. The data acquisition process was synchronized with the valve drive waveforms and ensemble-averages over many blowing cycles were taken to minimize the effect of noise.

The data acquisition system also generated the valve drive waveforms.

Validation of the complete system was achieved by comparing loads (without blowing) with those obtained for the same model and test conditions in previous tests at a different facility. The results agreed very well.

3.4 Flow Visualization

To gain a better understanding of the underlying flow phenomena, the force and moment data were complemented by surface and off-surface flow visualization. The surface flow visualization studies were performed in the wind tunnel using a mixture of titanium dioxide and vacuum pump oil spray-coated over the entire surface of the forebody portion of the model. Testing was conducted at $\alpha=45$ deg for velocities of 18.3 and 36.6 m/s. The surface skin friction patterns were permitted to evolve in the presence of either steady port or steady starboard blowing.

Off-surface visualization experiments were conducted in the water tunnel at the University of Ottawa[6]. Due to the smaller size of this facility, tests were performed on the isolated forebody of the model (i.e., no wing or tail). This was deemed acceptable because the main reason for the tests was to gain a better understanding of the flow in the vicinity to the forebody apex. The flow was visualized by injecting dye into the flow upstream of the model tip and/or into the nozzle flow.

4 Results and Discussion

Results are presented in non-dimensional form as coefficients of time-average yawing moment (\overline{C}_n), side force (\overline{C}_Y), pitching moment (\overline{C}_m), normal force (\overline{C}_Z), and rolling moment (\overline{C}_l). The uncertainties for these measurements are respectively ± 0.0015 , ± 0.0035 , ± 0.0065 , ± 0.025 , and ± 0.002 . The sign convention for the moments and forces are shown in Fig. 3. The coefficient of blowing momentum is considered positive when air is applied through the starboard nozzle, and negative through the port nozzle. Nozzle blowing was always asymmetric, that is, blowing was applied to either the starboard or port nozzle, not

both at the same time. The uncertainty of C_μ is about ± 0.0001 .

4.1 Effect of C_μ

The effect of C_μ on the time-average yawing moment coefficient, \overline{C}_n , is depicted in Fig. 6 for $\alpha=45$ deg. For $C_\mu < 0.0013$, positive C_μ (starboard blowing) causes negative \overline{C}_n indicating that the port forebody vortex is attached while the starboard vortex is detached. This is as one might expect, that is, the perturbation due to starboard blowing causes detachment of the starboard vortex. However when C_μ exceeds about 0.0025, \overline{C}_n has the same magnitude as before, but is positive, indicating that the forebody vortices have switched to the other stable arrangement. The corresponding behaviour is observed for port blowing. The water-tunnel flow visualization, see Fig. 7, showed that this ‘reversal’ phenomenon coincided with penetration of the shear layer by the fluid issuing from the blowing nozzle. That is, for C_μ somewhat above the ‘reversal threshold’ of about 0.0013 the blowing fluid forms a free jet which penetrates through the shear layer and emanates from the forebody when it is at high α . This flow condition apparently favours attachment of the vortex formed on that side of the forebody.

The reversal phenomenon was not observed in the earlier tests perhaps due to the larger apex semi-angles of those models (30 deg). In practical applications C_μ would have to be either well below or well above the threshold value if reversal occurs for the particular forebody. It is noteworthy that a C_μ of only about 0.0004 is required to reliably switch the vortex arrangement.

The behaviour and magnitude of \overline{C}_n and the other aerodynamic coefficients are essentially the same for C_μ either above or below the reversal threshold. All subsequent data in this paper are for C_μ above the threshold.

4.2 Steady Blowing

Figure 8 shows the effect of angle of attack on time-average moments and forces with steady blowing through either the port or starboard noz-

zle. The variation with α is highly non-linear and for \bar{C}_n , \bar{C}_Y and \bar{C}_ℓ it reflects the fact that forebody vortices are present and asymmetrically positioned in one of two possible stable arrangements over the range $30 < \alpha < 60$ deg. The presence of a significant baseline \bar{C}_n and \bar{C}_Y (i.e., no blowing) for $\alpha > 25$ deg serves as evidence of an inherent asymmetry in the vortex positions. Clearly the vortex arrangement is controlled by the blowing and signs are consistent with C_μ above the reversal threshold. The responses to port and starboard blowing are seen to be nearly symmetrical although the side force results appear to be slightly offset from $\bar{C}_Y = 0$. In view of the good symmetry of \bar{C}_n , which is largely the result of forces acting on the forebody, the asymmetry in \bar{C}_Y may be due to side force contributions acting near the moment reference centre.

The non-zero rolling moment seen in Fig. 8 is presumably due mainly to the influence of the forebody vortices on the flow over the wings. Steady nozzle blowing has only a small influence on \bar{C}_Z and \bar{C}_m (not shown).

4.3 Dynamic Blowing

The effect of duty cycle τ/T (see Fig. 1) on time-average forces and moments is shown in Fig. 9 for various α values. Time-average yawing moment varies linearly in accordance with the expectations of Fig. 1(b). For $\alpha = 45$ deg the symmetry and linearity in the variation of \bar{C}_n is particularly good. The magnitudes of \bar{C}_n under steady blowing conditions ($\tau/T = 0\%$ and 100%) are in good agreement with each other. Time-average side force is very small compared to the normal force, \bar{C}_Z , and trends in the data are unclear due to poor signal-to-noise ratio. The principal difference from the previous experimental results (Fig. 2) is the reversed slope of the linear variation. This is a consequence of the aforementioned reversal phenomenon since the C_μ of Fig. 9 exceeds the reversal threshold. The variation of \bar{C}_n with duty cycle remains reasonably linear as the angle of attack, α , is changed. The dependence on α reflects the behaviour seen in Fig. 8(a).

Dynamic manipulation of the forebody vor-

tices also affects forces and moments about other axes as seen in Fig. 9(c)-(e). Consistent with Fig. 8(c), in Fig. 9(e) an approximately linear variation of \bar{C}_ℓ with duty cycle is seen to exist for α near 40 deg. At 50% duty cycle, \bar{C}_ℓ is not precisely zero, but it is much less than for naturally-occurring asymmetric vortices. This result confirms an earlier finding that alternating blowing using a 50% duty cycle has the potential to eliminate asymmetric rolling moments due to forebody vortex asymmetry[7].

For the most part the variation of τ/T was found to have a small effect on \bar{C}_m and \bar{C}_Z . As seen in Fig. 9(d), however, the results for \bar{C}_Z show an interesting gain at some α values for alternating blowing as opposed to steady blowing. This is particularly evident for $\alpha = 35$ deg and $\tau/T = 50\%$ where the increase is about 15%. It appears that this effect results from the influence of the forebody vortices on the wing leading-edge vortex breakdown locations, which largely depend on the relative position of the corresponding vortices on each side. Under alternating blowing conditions, the varying interaction between the forebody and leading-edge vortices leads to a corresponding modulation of the latter's breakdown locations. It is known that the aft propagation speed of breakdown is considerably higher than its forward propagation speed[8], thus, under dynamic conditions, the average location of breakdown is further aft than the corresponding static value, leading to the observed increase in normal force.

4.4 Effect of Sideslip

The effect of sideslip on the variation of time-average forces and moments with duty cycle is seen primarily in the results for \bar{C}_n and \bar{C}_m at $\alpha \simeq 45$ deg in Fig. 10. It is clear that nozzle blowing continues to be effective with non-zero sideslip. The results presented are for a tip that has the nozzle cutout as close to the apex as practicable ($x_n/D = 0.095$, $\theta = 120$ deg). In fact the nozzle exit is even closer to the apex than for the tip shown in Fig. 4. It is thought that the large ratio of nozzle diameter to the local cross-sectional radius of the forebody is primarily responsible for

the continued effectiveness with sideslip. With a large ratio, the fraction of forebody surface area removed by the nozzle cutout is significant, allowing the nozzle flow to continuously influence the local shear layer separation process, in spite of the circumferential movement of the primary separation line caused by sideslipping.

The variation of \bar{C}_n remains linear with duty cycle under sideslipping conditions. The curves for different β values are approximately parallel; the same is true of the rolling moment curves (not shown). This indicates that the effects of sideslip can simply be superimposed onto those due to τ/T . In Fig. 10(a), $\partial\bar{C}_n/\partial\beta$ is negative, indicating directional instability, as would be expected at high angles of attack due to blanketing of the vertical tail. Figure 10(b) reveals a cross-coupling effect between \bar{C}_m and τ/T . Specifically, sideslip gives rise to a linear variation of \bar{C}_m with τ/T . This is thought to be due to a shifting centre of pressure for \bar{C}_Z , associated with β -induced lateral position shifts of the forebody vortices.

4.5 Effect of Longitudinal Nozzle Placement

Figure 11 illustrates the effect of longitudinal position of the nozzles on blowing effectiveness. The nozzles in Tip 2-2 are located closer to the apex of the forebody than those of Tip 1-7, though both are placed along the same meridian ($\theta = 135$ deg). Tip 2-2 yields slightly different results but the differences are not major. The comparison in Fig. 11 is incomplete, however, because of the absence of results for a third tip which has the farthest aft nozzle location. Measurements were not taken for this tip at $\alpha > 40$ deg due to a high risk of encountering unacceptable model vibration[9].

4.6 Effect of Azimuthal Nozzle Placement

Figure 12 shows the effect of circumferential position of the nozzles on blowing effectiveness. The results presented pertain to three tips, the nozzles of which are located at the same axial station. In general, there does not appear to be any major difference in the magnitude of \bar{C}_n and the other aerodynamic coefficients due to the varia-

tion of the circumferential location of the nozzles. Again, this may be due to the relatively large ratio of nozzle diameter to local radius of the forebody cross-section. Given the same nozzle diameter on a model with a larger apex semi-angle, hence a larger local radius, a more substantial influence of circumferential location may occur.

5 Concluding Remarks

A scheme has been proposed to obtain a linear variation of yawing moment and side force by means of dynamic manipulation of forebody vortices. The concept involves the oscillatory perturbation of the flowfield near the forebody apex and it has the potential to overcome the problems associated with steady vortex control methods. Results from wind-tunnel tests using a schematic aircraft model with forward blowing as a means of perturbing the vortices, have shown that the proposed method of control is feasible with realistic aircraft configurations. Significant differences were found to exist between the current results and those obtained with an earlier ogive-cylinder model. With the most recent results, the signs of \bar{C}_n and \bar{C}_Y were found to change when the nozzle blowing momentum exceeded a certain threshold value. Linearity of \bar{C}_n with duty cycle is still observed, however. Axial and circumferential position of the blowing nozzles have only minor effects on results over the range investigated.

With an aircraft configuration, cross-coupling effects on the roll and pitch axes are to be expected and were indeed observed. One notable result was a gain in \bar{C}_Z that occurs with a 50% duty cycle and zero sideslip.

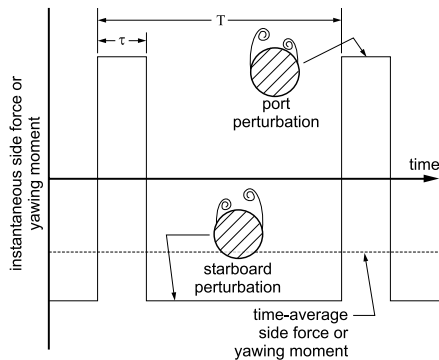
References

- [1] Malcolm, G.N. Forebody vortex control - a progress review. AIAA Paper 93-3540-CP, August 1993. pp. 1082-1116.
- [2] Williams, D. A review of forebody vortex control scenarios. AIAA Paper 97-1967, June 1997.
- [3] Alexan, K., Hanff, E.S., and Kind, R.J. Water-

APPLICATION OF DYNAMIC MANIPULATION OF THE FOREBODY VORTICES ON A SCHEMATIC AIRCRAFT MODEL

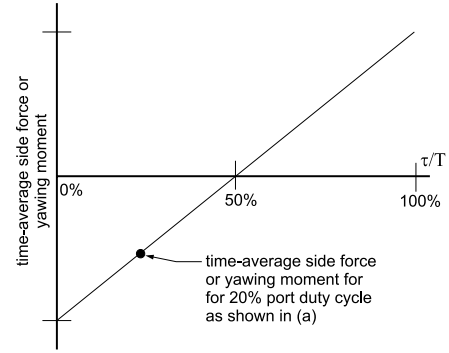
tunnel investigation of dynamic manipulation of forebody vortices. AIAA Paper 94-0503, January 1994.

- [4] Lee, R., Hanff, E.S., and Kind, R.J. Wind-tunnel investigation of dynamic manipulation of forebody vortices. AIAA Paper 95-1794, June 1995.
- [5] Pope, A. and Rae, W. *Low-Speed Wind Tunnel Testing*. Wiley, New York, second edition, 1984.
- [6] Dunn, W.R., Tavoularis, S., and Lee, B.H.K. Visualization of flow past a model of a fighter aircraft in a water tunnel. In *CD-ROM Proceedings, 8th International Symposium on Flow Visualization*, Paper 63, Sorrento, Italy, 1-4 September 1998.
- [7] Ng, T.T., Suarez, C.J., Kramer, B.R., Ong, L.Y., Ayers, B., and Malcolm, G.N. Forebody vortex control for wing rock suppression. *Journal of Aircraft*, Vol. 31, No 2, pp 298–305, March-April 1994.
- [8] Hanff, E.S. and Huang, X.Z. Roll-induced crossloads on a delta wing at high incidence. AIAA Paper 91-3223, September 1991.
- [9] Lee, R., Hanff, E.S., and Kind, R.J. Active control of forebody vortices on a schematic aircraft model. In *RTO Meeting Proceedings, Active Control Technology for Enhanced Performance Operational Capabilities of Military Aircraft, Land Vehicles and Sea Vehicles*, Symposium on Performance, Stability and Control, Fluid Physics (PSF), Session V, Paper 22, Braunschweig, Germany, 8-11 May 2000.



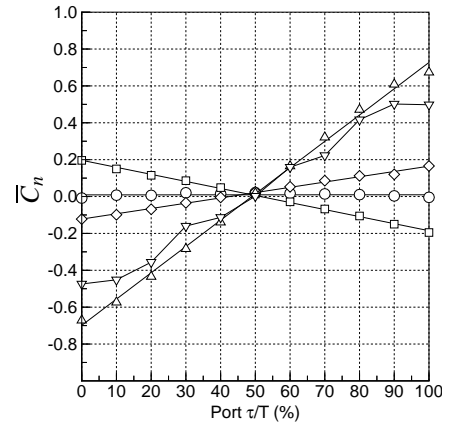
(a) Idealized side force or yawing moment time-history.

Fig. 1 : Principle of the dynamic manipulation of forebody vortices.

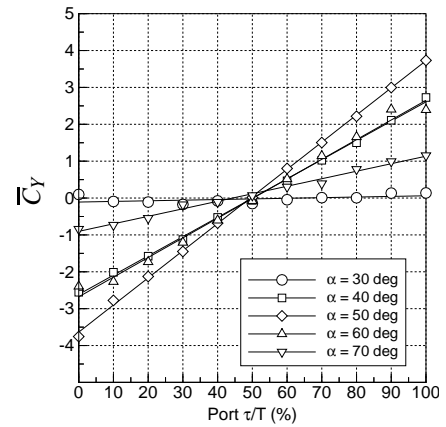


(b) Expected variation of time-average side force or yawing moment with duty cycle.

Fig. 1 : (continued)



(a) Yawing moment



(b) Side force

Fig. 2 : Variation of \bar{C}_Y and \bar{C}_n with duty cycle for an ogive-cylinder model. $C_\mu = 0.00066$, $Re_D = 1.76 \times 10^5$ (19.2 m/s), $\omega^* = 0.32$ (7.2 Hz), $\beta = 0$ deg. The moment reference center is $3.5D$ aft of the forebody apex. (Ref. [4])

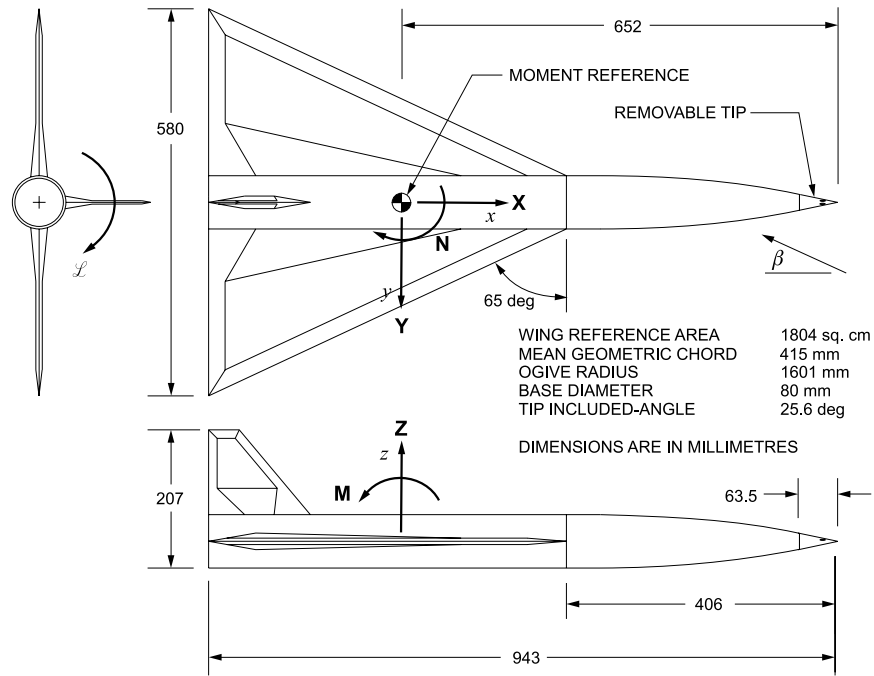


Fig. 3 : 65-deg delta-wing model with a long, slender forebody of circular cross-section, featuring a removable tip. Forces, moments, and angles are positive as shown.

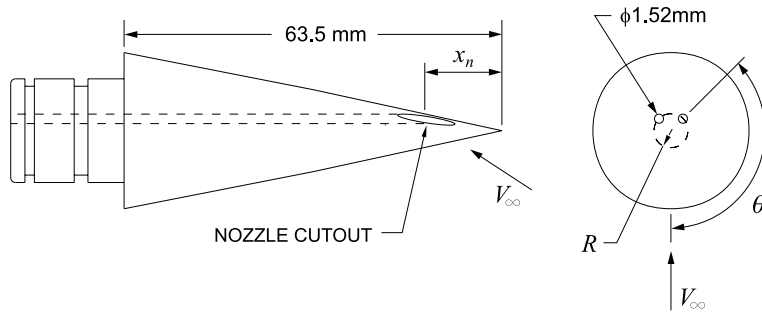


Fig. 4 : Schematic of removable forebody tip. For the tip shown, $x_n/D = 0.159$ and $\theta = 135$ deg.

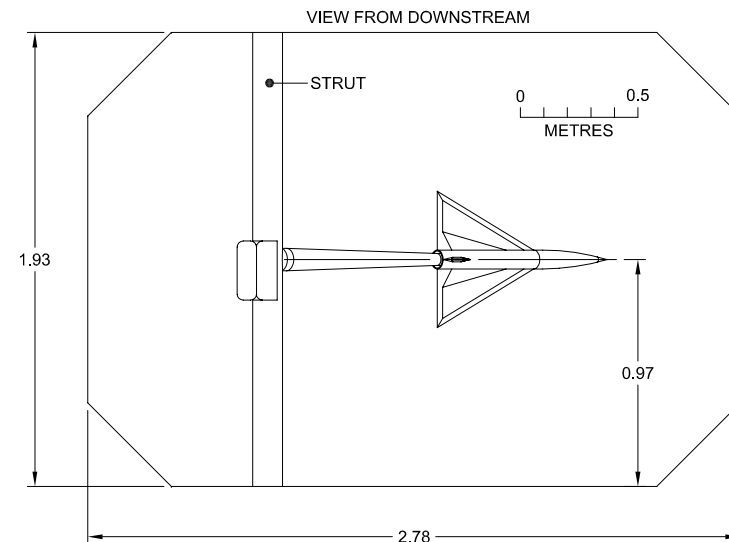
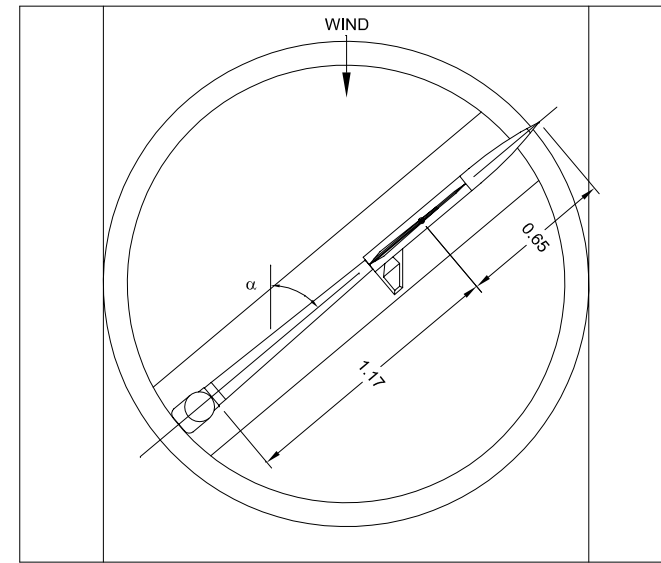


Fig. 5 : Two views of the model installation in the working section of the 2m x 3m wind tunnel.

APPLICATION OF DYNAMIC MANIPULATION OF THE FOREBODY VORTICES ON A SCHEMATIC AIRCRAFT MODEL

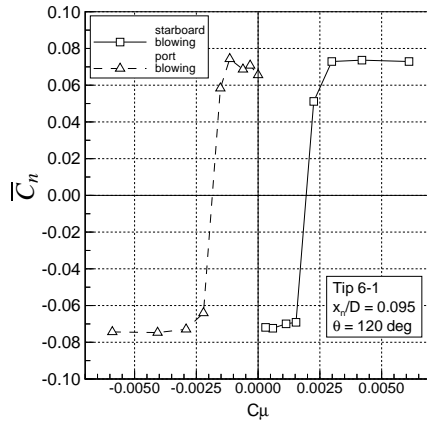
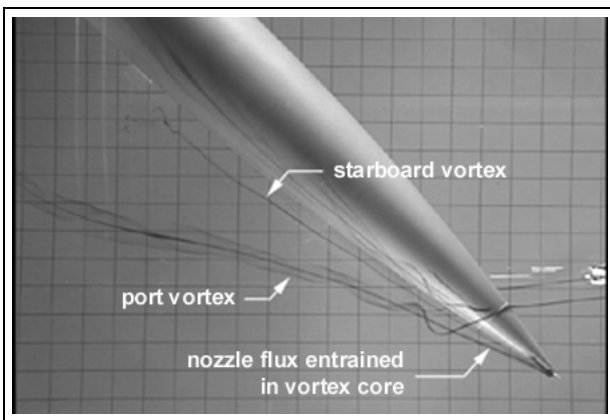
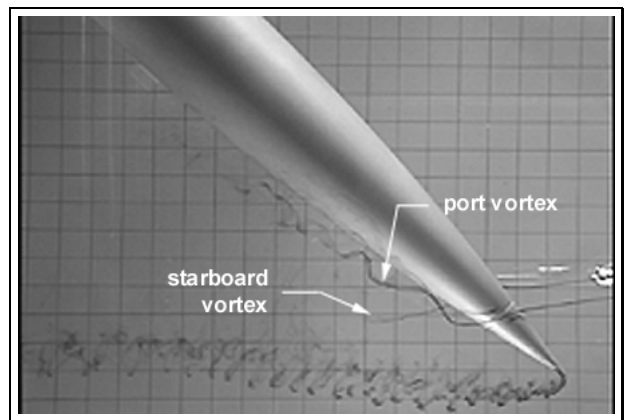


Fig. 6 : Variation of \bar{C}_n with steady blowing moment coefficient. $Re_D = 1.96 \times 10^5$ (36.6 m/s), $\alpha = 45$ deg, and $\beta = 0$ deg. Positive C_μ denotes starboard blowing.



(a) Port blowing with C_μ below reversal threshold; nozzle flux entrained into port forebody vortex which is detached, starboard attached; \bar{C}_n and \bar{C}_Y are positive.



(b) Port blowing with C_μ above reversal threshold; port forebody vortex is attached, starboard detached; \bar{C}_n and \bar{C}_Y are negative.

Fig. 7 : Water-tunnel flow visualization using dye injection on the isolated forebody (port view). $\alpha = 45$ deg, $Re_D = 4.44 \times 10^3$.

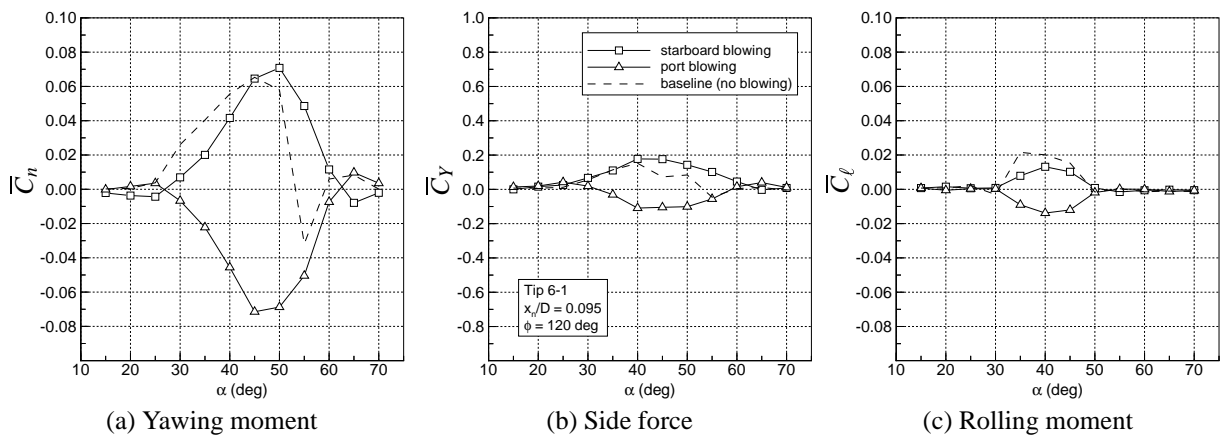


Fig. 8 : Variation of time-average forces and moments with angle of attack for steady blowing. $C_\mu = 0.00264$, $Re_D = 1.96 \times 10^5$ (36.6 m/s), and $\beta = 0$ deg.

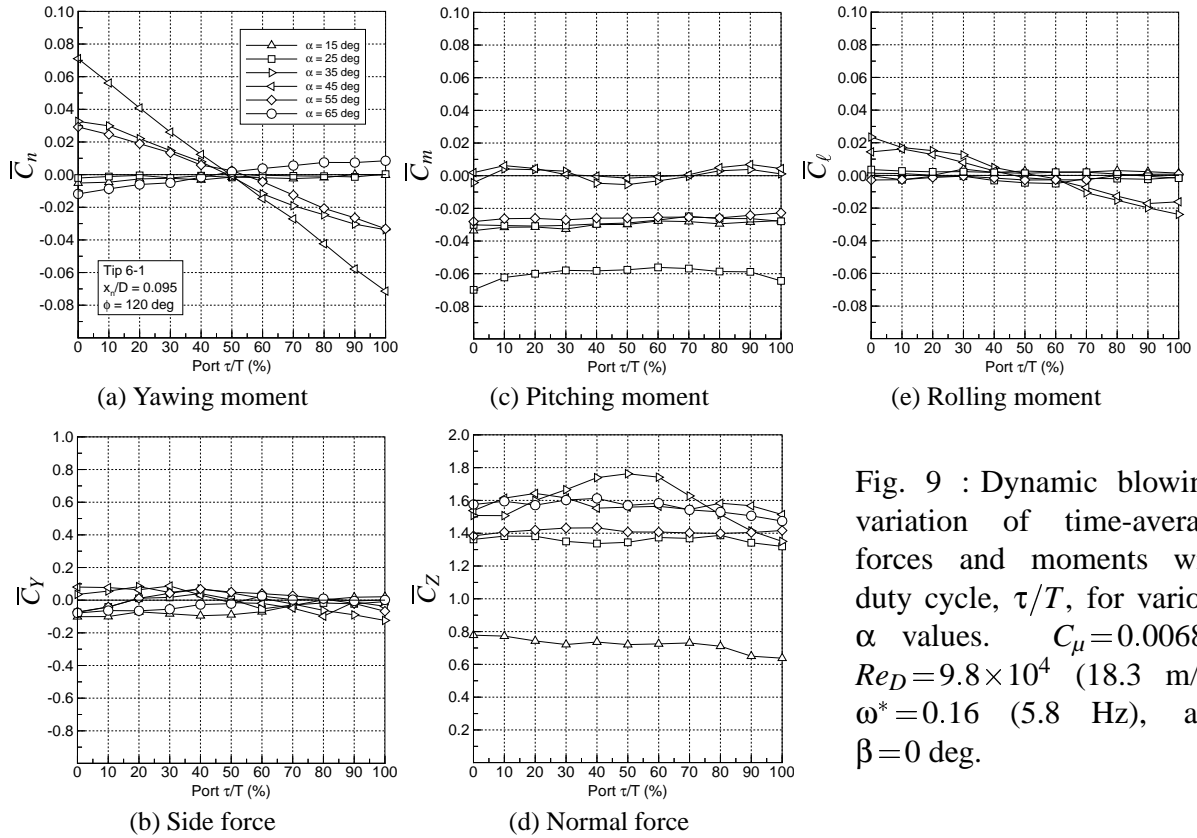


Fig. 9 : Dynamic blowing; variation of time-average forces and moments with duty cycle, τ/T , for various α values. $C_\mu=0.00686$, $Re_D=9.8 \times 10^4$ (18.3 m/s), $\omega^*=0.16$ (5.8 Hz), and $\beta=0$ deg.

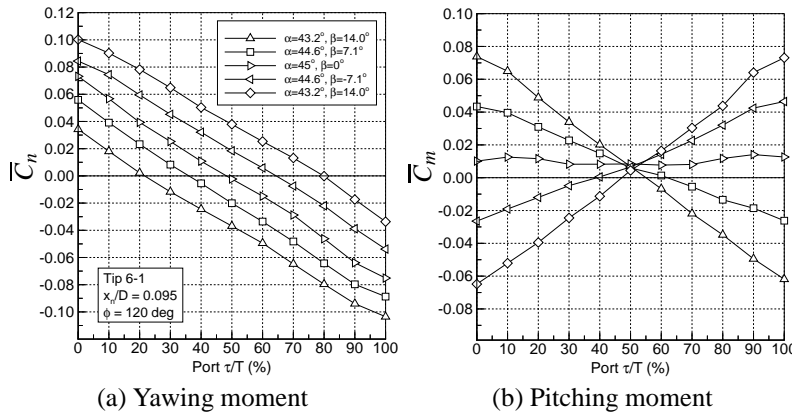


Fig. 10 : Effect of sideslip on the variation of \bar{C}_n and \bar{C}_m with duty cycle. $C_\mu=0.00351$, $Re_D=2.0 \times 10^5$ (36.6 m/s), $\alpha=45$ deg, $\omega^*=0.16$ (11.6 Hz).

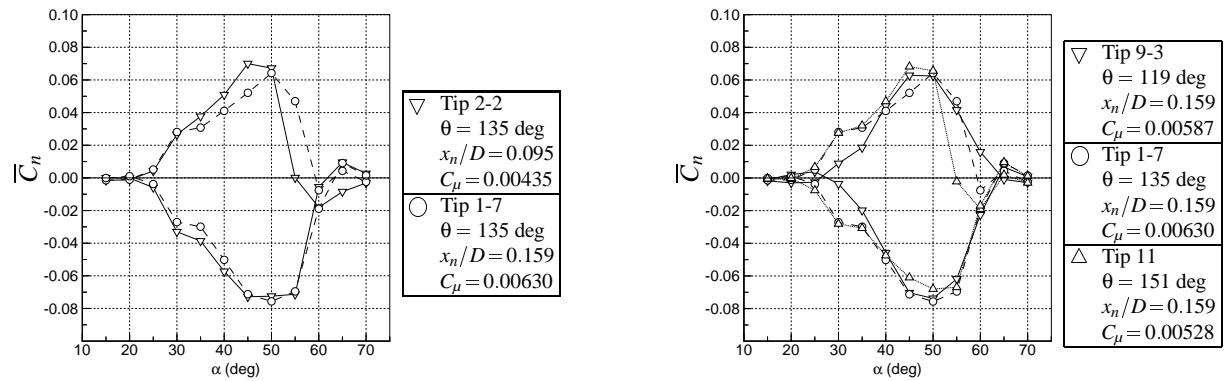


Fig. 11 : Effect of longitudinal position of nozzles on blowing effectiveness for steady blowing. $Re_D=1.94 \times 10^5$ (36.6 m/s), $\beta=0$ deg.

Fig. 12 : Effect of circumferential position of nozzles on blowing effectiveness for steady blowing. $Re_D=1.95 \times 10^5$ (36.6 m/s), $\beta=0$ deg.